Ind. J. Pharm. Edu. Res., 2023; 57(2s):s301-s306.
https://www.ijper.org

Original Article

Biofabrication and Characterization Using Egg Shell Nanoparticles and their Haemolytic Analysis: An *in-vitro* Study

Dinesh Y*, Satheesh Kumar Balu, Karthikeyan Ramalingam, Pratibha Ramani

Department of Oral and Maxillofacial Pathology, Saveetha Dental College and Hospital, Saveetha Institute of Medical and Technical Sciences, Chennai, Tamil Nadu, INDIA.

ABSTRACT

Aim/Background: Hydroxyapatite is a bioactive, biocompatible, and osteoconductive component having similar chemical characteristics to bone and tooth mineral components. Due to its porous structure and resistance to high temperatures, hydroxyapatite is commonly used as a catalyst and adsorbent. Eggshells are abundant in calcium carbonate, calcium phosphate, and other organic chemicals, making them excellent for CaO production. **Materials and Methods:** ES-Hap NPs from eggshell through an oil-bath-mediated precipitation technique. Egg shell nanoparticles were manufactured using chemical reagents like ammonia in a silicone oil bath. Preparation using a series of chemical reagents and characterization were done; functional groups were analysed using FTIR; and morphological analysis was analysed using FESEM. Hemolysis analysis was also done. **Results:** FTIR analysis showed functional PO_4 groups, for the ES-Hap NPs at 1015 cm^{-1} and 563 cm^{-1}, respectively. The XRD results based on crystallinity demonstrated Hap NPs of 20.86 nm. A FESEM investigation established the dimensions of NRs to be 78.15 nm and 221.62 nm, respectively. Crystallite size demonstrated that Hap NPs are comparable to normal human bone and may be employed as regenerative therapies. In addition, the hemolysis testing demonstrated superior blood compatibility compared to chemically manufactured, traditional Hap. **Conclusion:** These biogenic ES-Hap NPs can be further analysed for antimicrobial properties and *in vivo* studies, which could be highly beneficial for medical applications.

Keywords: Egg shell, Nanoparticles, Hemolytic analysis, XRD, FTIR, FESEM.

Correspondence:
Dr. Dinesh Y
Postgraduate Student, Department of Oral and Maxillofacial Pathology, Saveetha Dental College and Hospital, Saveetha Institute of Medical and Technical Sciences, Chennai, Tamil Nadu, INDIA.
Email: drdineshdentist@gmail.com
ORCID ID: 0000-0001-5535-0356

Received: 29-12-2022;
Revised: 17-01-2023;
Accepted: 02-03-2023.

INTRODUCTION

The most adaptable inorganic biomaterial utilised in biomedicine is Hydroxyapatite (Hap). It is a calcium phosphate mineral that naturally occurs in the apatite family. Currently several biomaterial research on bone regeneration, hard tissue replacement and reconstructive materials. $Ca_{10}(PO_4)_6(OH)_2$, commonly known as hydroxyapatite, is a white solid compound with a hexagonal structure.[1] Hydroxyapatite is a bioactive, biocompatible, and osteoconductive component having similar chemical characteristics to bone and tooth mineral components.[2] As a result, hydroxyapatite is accepted in several studies as a bone and dental implant filler and coating material. Due to its porous structure and resistance to high temperatures, hydroxyapatite is commonly used as a catalyst and adsorbent.[3]

DOI: 10.5530/ijper.57.2s.34

$Ca(NO_3)_2$, $Ca(OH)_2$, $CaCO_3$, or bio-organic materials such as animal bone, egg shell etc can be used to prepare synthetic hydroxyapatite.[4] Human bone is composed of inorganic components (70%) $CaPO_4$ and organic components (30%).[5,6] Hydroxyapatite is a mineral that is both highly bioactive and biocompatible with human organs. Because of its propensity to make chemical connections with hard tissue, it has gained great attention in biological science.[7]

Hap's corrosion resistance, non-carcinogenic, biocompatible and bone regenerative properties and can be used in a variety of bone defects. Stainless Steel and titanium are quite commonly used in implant materials in the production of load-bearing bone regeneration. Researchers are interested in bioactive and bioinert materials to replace metallic implants due to issues with their functionality in the human body and their endurance over time. Hap has generated considerable attention in orthopaedic applications. Hap not only forms a chemical bond with a bone, but it also relieves pain caused by weight bearing. In spite of this, hydroxyapatite has several additional important uses, such as dental applications, biomedical research etc.[8,9]

Numerous researchers have tried to synthesise the Hap in various methods. Traditional techniques for manufacturing Hap include wet precipitation, hydrothermal approach, sol-gel technology etc were used.[4] Numerous techniques need calcination at 1200°C in order to produce the final Hap phase, while others are very time-consuming and result in the creation of undesirable anions. Several studies have utilised eggshell in the chemical production of Hap.[10]

Every day, an enormous amount of eggshells are discarded since they are worthless. These eggshells foster microbial growth and are detrimental to the environment. The food processing industry produces around 250,000 tonnes of eggshell annually. About 11% of an egg's entire weight is eggshell. These eggshells are abundant in calcium carbonate (91 to 94%), calcium phosphate (1%), and other organic chemicals, making them excellent for CaO production.[11] In this study, an attempt was made to use eggshell waste as a calcium source for the production of ultrapure and nanocrystalline Hap powder. The manufactured ES-Hap NPs powder was characterised utilising XRD, FESEM, FTIR and hemolytic analysis was also done.

MATERIALS AND METHODS

Egg shells (ES) was collected and treated using $(NH4)_2HPO_4$ and ammonia solution. Reaction temperature maintained using an oil bath. Compared to a water bath, silicone oil was utilized at 30 to 250°C due to its high temperature and oxidation stability, as well as its capacity to maintain a constant temperature for an extended length of time.[2] After annealing, the ES-Hap NPs' colour changes from white to light grey and the organic molecules are removed.

Chemicals and Reagents

Calcium-rich chicken egg shells were collected from Koyambedu market in Chennai, Tamil Nadu, India. All of the chemicals utilised in this study includes $(NH_4)_2HPO_4$, C_3H_6O, NH_4OH, and C_4H_8 were analytic grade.

Preparation of egg shell powder

The thick egg shell was cleaned using a series of reagents such as distilled water, ethanol and acetone. Hot air oven was used for drying at 60°C for 24 hr, and 20 g of egg shells were crushed for 5 hr in a high-energy ball mill. For future investigation, the powder was kept in a desiccator inside a sterile plastic container at room temperature.

Preparation of Egg Shell-Hap nanoparticles

During Hap synthesis, the temperature of an oil bath was controlled using a magnetic stirrer. Using a burette, 1 molar (1.008 g) of egg shell powder was added to a round-bottomed flask, and then $(NH_4)_2HPO_4$ was added. At this stage, pH was adjusted to 8–12 pH units (Thermo Scientific, Model EcoTester). During synthesis, the temperature of an oil bath was managed using a magnetic stirrer. agitated at 80°C for 24 hr before being washed with ethanol and distilled water to remove contaminants.[4]

The precipitate was then dried in an oven with hot air at 60°C before being ground into a powder. Annealing was done at 700°C for six hours, and characterization of ES-Hap NPs was done. In order to evaluate the morphology of nanomaterials, it is vital to adjust variables such as duration, temperature, pH, and concentration of reagents.[12]

Characterization of Egg Shell-Hap Nanoparticles by X-ray Diffraction

Using an X-ray powder diffractometer, X-ray diffraction (XRD) was conducted on Hap nanorods to examine their crystallinity and phase evolution (Bruker, Model D8 Advance). ES-Hap NP powder were crushed and powdered using graphite and pestle. Comparing the results to conventional XRD patterns from JCPDS revealed and corroborated the crystallite size and phase development of the eggshell-bone-derived Hap nanoparticles.

Fourier-transform infrared spectroscopy

FTIR-spectrometer (Perkin Elmer Spectrum model) analysed for functional groups in eggshells, and eggshell-derived Hap nanoparticles were detected. The sample container was immediately filled with ES powder (ball milled) and ES-HAP NP powders that were synthesised. The sample was scanned in Attenuated Total Reflectance (ATR) mode from 4000 to 500 cm^{-1}.

Field emission scanning electron microscopy (FESEM)

Micrographs taken in FESEM (JEOL, Japan) of ES-Hap NPs operating at 200 kV A sufficient sample was applied over a carbon coated copper grid, and its size and shape were characterized. Using ImageJ software, the average particle size distribution of ES-Hap NPs was displayed.

Hemolysis assay

The blood donor consented to the test with full knowledge. A healthy volunteer's blood was extracted by a physician and mixed in a 1:10 ratio with 3.2% trisodium citrate to avoid clotting. To make ES-Hap NPs at various concentrations (200, 100, 75, 50, 25, and 10 g/mL), freshly prepared phosphate buffer saline was used, and anticoagulated blood was used as the test material.as positive and negative controls, anticoagulated blood with 0.1% sodium carbonate and anticoagulated blood with PBS, respectively.

Before being centrifuged at 2000 rpm for 5 min, all test samples and controls were incubated at 37°C for 3 hr. The Optical Density (OD) of the supernatant was measured at 540 nm. To ensure reproducibility, each experiment was conducted in triplicate. The formula used to calculate the blood compatibility percentage Blood compatibility analyses were done at various concentrations; the hemolytic activity of ES-Hap NPs was calculated. Membrane

damage due to crystals and erythrocyte clumping was assessed with the addition of Hap microcrystals in blood.[8]

The ES-Hap NPs demonstrated good results of non-hemolytic to RBS with a score of less than 2% hemolysis up to 75 g/mL. In addition, when higher concentrations of ES-Hap NPs, such as 100 and 200 g/mL, were applied to blood samples, 2% and 3.2% hemolytic activity, respectively, were observed. This shows that at higher concentrations of ES-Hap NP, nanorods may have minimal hemolytic activity. The enhanced hemolytic activity due to oxidative stress on the addition of ES-Hap nanoparticles to blood cells.[13]

RESULTS

Our study showed XRD pattern of calcium carbonate shows the diffraction peaks obtained at 26°, 30°, 32°, 33°, 35°, 38°, 46°, 47°, and 52° correspond to the (003), (212), (116), (303), (204), (316), (225), and (002) planes, indicating that Hap formed a hexagonal structure (Figure 1). The IR bands obtained for the ES-Hap sample at 1015 cm^{-1} and 563 cm^{-1}, respectively, indicate that the FTIR analysis revealed functionally asymmetric and symmetric PO_4 stretching groups (Figure 2). This insight contributes to the evaluation of the ES-Hap nanorod production. The rod morphology of ES Hap NPs is visible in FESEM micrographs at various magnifications. Using ImageJ software, the width and length of the nanoparticles were found to be 78.5 in 0.44 nm and 218.98 in 0.36 nm, based on FESEM (Figures 3 and 4). The addition of Hap crystals to blood will result in hemolysis due to erythrocyte clumping and crystal-induced damage. However, up to 75 g/mL of ES-Hap NPs displayed less than 2% hemolysis, indicating nonhemolytic. When a larger quantity of ES-Hap NPs, 100 g/mL and 200 g/mL mixed with blood and hemolytic activity increased to 2.2% and 3.2%, respectively (Figure 5).

DISCUSSION

Crystallinity and phase formation analysis

Powder XRD was used to analyse the products formed and the egg shell powders, demonstrating that a longer reaction time results in the development of highly crystalline Hap nanorods.[14] Our study showed XRD pattern of calcium carbonate shows the diffraction peaks obtained at 26°, 30°, 32°, 33°, 35°, 38°, 46°, 47°, and 52° correspond to the (003), (212), (116), (303), (204), (316), (225), and (002) planes, indicating that Hap formed a hexagonal structure. Balu *et al.* 2020 report reveals that, after 3 hr of reaction, aragonite $CaCO_3$ was entirely changed into calcite $CaCO_3$.[15] Basic pH and 80°C temperature facilitates the 3 hr relaxing of aragonite calcium carbonate links to produce calcite structure.[16] Based on the diffraction peaks, the production of Hap crystals and traces of calcite began to appear after 6 hr of reaction time. In addition, when response time increased, the intensity of calcite at peak points 23° and 29° reduced dramatically. At increasing duration at 48hr, the calcite peak vanished as a result of the full creation of Hap. Despite the formation of Hap XRD peaks after 24 hr, crystalline structures were formed.[17]

Evaluation of functional groups

Functional groups present in the ES-Hap NPs were analysed using FTIR.[18] FTIR-spectra of ES-Hap NPs with high crystallinity, which is necessary to examine their functional groups.[19,20] This insight contributes to the evaluation of the ES-Hap nanorod production.[21] According to earlier research, there are two categories of carbonate substitutions on Hap, including A-type substitutions that occur at the O-H vibrational site and B-type substitutions that occur at phosphate vibrational sites. Due to this, the band at 1450 cm^{-1} denoting the B-type carbonates,

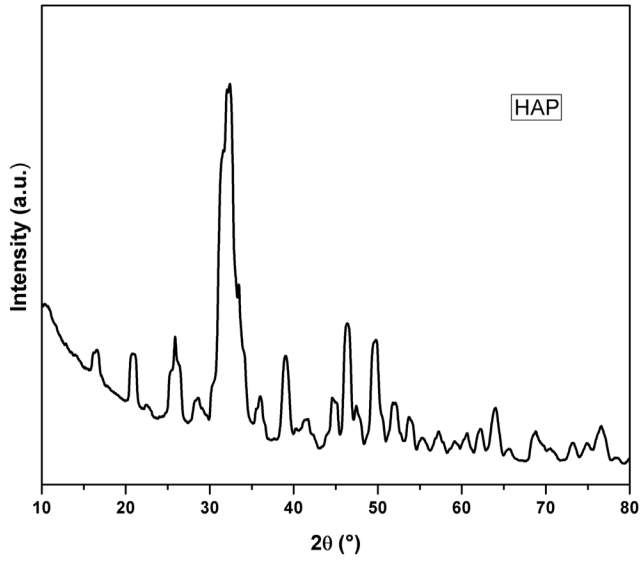

Figure 1: Graph representing the crystallinity and phase formation analysis using XRD of intensity of Hap NPs in a.u.

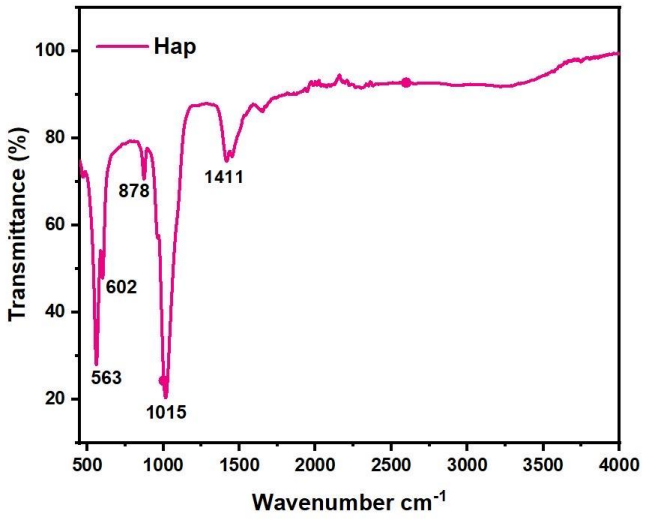

Figure 2: Graph showing FTIR analysis data of transmittance % with respect to wave number cm^{-1}.

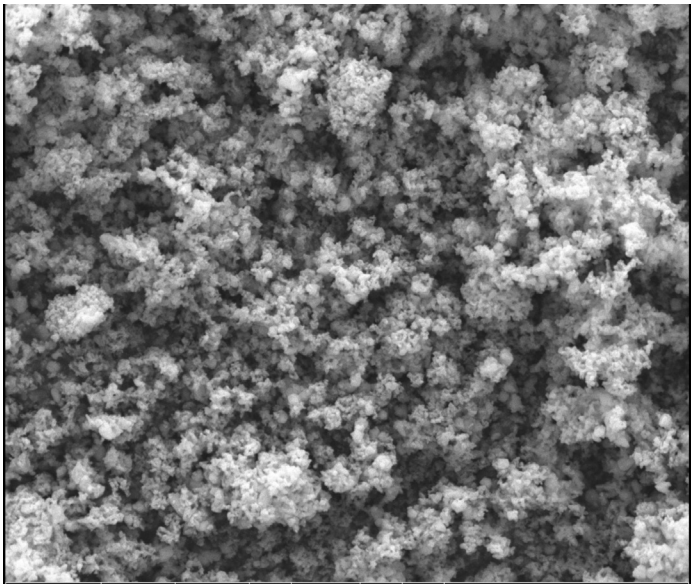

Figure 3: FESEM micrograph at 20,000x magnification.

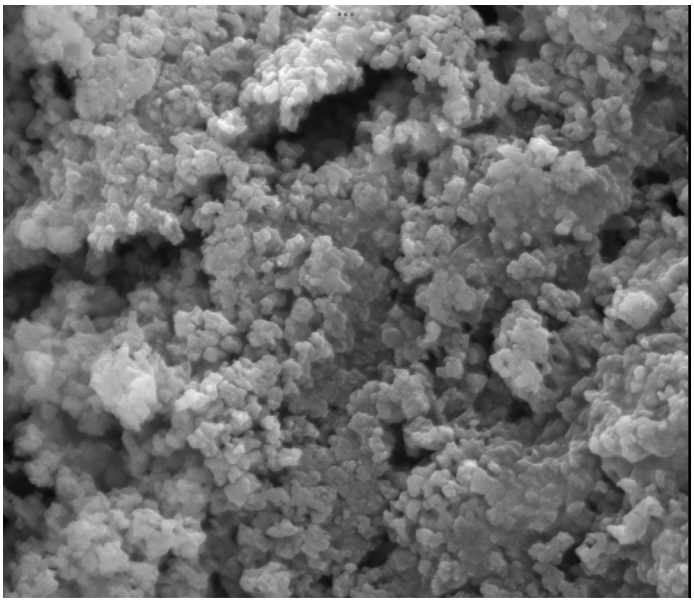

Figure 4: FESEM micrograph at 60,000x magnification.

and carbonated n-Hap, have its role in the regeneration of hard tissues.[22-24]

Morphology and elemental analysis

FESEM micrographs revealing the form and dimensions of ES-derived Hap NPs manufactured at 80°C for 48 hr. The rod morphology of ES Hap NPs is visible in FESEM micrographs at various magnifications. Similarly fabrication of Hap nanorods by Kumar *et al.* with a width of 40–60 nm and a length of 500–700 nm using discarded snail shells and microwave irradiation.[25] A similar study by Padmanabhan *et al.* generated Hap NPs of a width of 70–90 nm and a length of 400–500 nm using the sol–gel process.[10] Similarly study by Papageorgiou manufactured Hap NPs of a width of 20 nm and a length of 400 nm using the hydrothermal technique. Thus, it is obvious from prior research that the

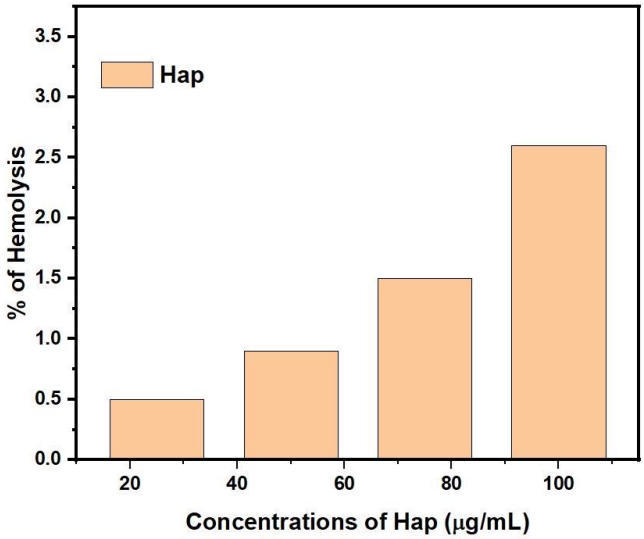

Figure 5: Hemolytic behaviour of Hap NPs using Egg shell powder as ES-Hap NPs analysing the % of hemolysis at various concentrations.

synthesis technique has a significant influence in modifying the size of Hap NPs, which ultimately defines their biological capabilities. However, based on FESEM images, nonporous Hap NPs may impact their biocompatibility. Consequently, the calcination temperature needs to be improved for enhancing tissue biocompatibility. Biocompatible non-toxic Hap nano rods are more advantageous for biomedical application.[11,26,27]

Hemolytic Analysis

The addition of Hap crystals to blood will result in hemolysis due to erythrocyte clumping and crystal-induced damage.[28] However, up to 75 g/mL of ES-Hap NPs displayed less than 2% hemolysis, indicating nonhemolytic. When a larger quantity of ES-Hap NPs, 100 g/mL and 200 g/mL mixed with blood and hemolytic activity increased to 2.2% and 3.2%, respectively. This shows that nanorods with a greater concentration of ES-Hap NR may display a minor hemolytic effect. ES-Hap nanorods and RBC interaction could have led to the oxidative stress thereby increasing concentration of hemolytic activity.[29,30] In addition, In the future, the hemolytic impact of large concentrations of ES-Hap NPs can be mitigated by optimising their surface charge.[9,31,32]

CONCLUSION

This study resulted in the preparation of ES-Hap NPs from eggshell through an oil-bath-mediated precipitation technique. To validate the characteristics of the eggshell-derived nanorods, the powders resulting from the precipitation process were examined using characterization techniques. The XRD results based on crystallinity demonstrated Hap NPs of 20.86 nm. A FESEM investigation established the dimensions of NRs to be 78.15 nm and 221.62 nm, respectively. Crystallite size demonstrated that Hap NPs are comparable to normal human bone and may be employed as regenerative therapies. In addition, the hemolysis

testing demonstrated superior blood compatibility compared to chemically manufactured, traditional Hap. These improved biological features of biocompatible Hap NPs add great value in the development of innovative orthopaedic and dental implants.

ACKNOWLEDGEMENT

We would like to thank the Research Lab in the Department of Oral Pathology at Saveetha Dental College and Hospital in Chennai for their support.

CONFLICT OF INTEREST

The authors declare that there is no conflicts of interests.

ABBREVIATIONS

ATR: Attenuated Total Reflectance; **ES-Hap NPs:** Egg shell hydroxyapatite nanoparticles; **FESEM:** Field emission scanning electron microscopy; **FTIR:** Fourier-transform infrared spectroscopy; **HA:** Hydroxyapatite; **Hap NPs:** Hydroxyapatite nanoparticles; **IR:** Infrared; **OD:** Optical Density; **XRD:** X-ray Diffraction.

SUMMARY

Eggshells are abundant in calcium carbonate, calcium phosphate, and other organic chemicals, making them excellent for CaO production. The manufactured ES-Hap NPs powder was characterized utilizing XRD, FESEM, FTIR and hemolytic analysis was also done. ES-Hap NPs from eggshell through an oil-bath-mediated precipitation technique. The IR bands obtained for the ES-Hap sample at 1015 cm^{-1} and 563 cm^{-1}, respectively, indicate that the FTIR analysis revealed functionally asymmetric and symmetric PO4 stretching groups. The XRD results based on crystallinity demonstrated Hap NPs of 20.86 nm. A FESEM investigation established the dimensions of NRs to be 78.15 nm and 221.62 nm, respectively. Hemolysis testing demonstrated superior blood compatibility compared to chemically manufactured, traditional Hap.

REFERENCES

1. Ponnulakshmi R, Shyamaladevi B, Vijayalakshmi P, Selvaraj J. *In silico* and *in vivo* analysis to identify the antidiabetic activity of beta sitosterol in adipose tissue of high fat diet and sucrose induced type-2 diabetic experimental rats. Toxicol Mech Methods. 2019;29(4):276-90. doi: 10.1080/15376516.2018.1545815, PMID 30461321.
2. Sundaram R, Nandhakumar E, Haseena BH. Hesperidin, a citrus flavonoid ameliorates hyperglycemia by regulating key enzymes of carbohydrate metabolism in streptozotocin-induced diabetic rats. Toxicol Mech Methods. 2019;29(9):644-53. doi: 10.1080/15376516.2019.1646370, PMID 31345080.
3. Alsawalha M, Rao CV, Al-Subaie AM, Haque SM, Veeraraghavan VP, Surapaneni KM. Novel mathematical modelling of Saudi Arabian natural diatomite clay. Mater Res Express. 2019;6(10). doi: 10.1088/2053-1591/ab2f9b.
4. Azis Y, Adrian M, Alfarisi CD, Khairat, Sri RM. Synthesis of hydroxyapatite nanoparticles from egg shells by sol-gel method. IOP Conf Ser.: Mater Sci Eng. 2018;345:012040. doi: 10.1088/1757-899X/345/1/012040.
5. Yu J, et al. Inhibitory effects of triterpenoid betulin on inflammatory mediators inducible nitric oxide synthase, cyclooxygenase-2, tumor necrosis factor-alpha, interleukin-6, and proliferating cell nuclear antigen in 1, 2-dimethylhydrazine-induced rat colon carcinogenesis. Pharmacogn Mag. 2020;16:836.
6. Hema SKH, Ramani P, Sherlin H, Sukumaran G, Jeyaraj G, Don KR, *et al*. Saliva as a diagnostic tool in oral squamous cell carcinoma–a systematic review with meta-analysis. Pathol Oncol Res. 2019;25(2):447-53. doi: 10.1007/s12253-019-00588-2, PMID 30712193.
7. Zafar A, Sherlin HJ, Jayaraj G, Ramani P, Don KR, Santhanam A. Diagnostic utility of touch imprint cytology for intraoperative assessment of surgical margins and sentinel lymph nodes in oral squamous cell carcinoma patients using four different cytological stains. Diagn Cytopathol. 2020;48(2):101-10. doi: 10.1002/dc.24329, PMID 31675175.
8. Elferink JG. Crystal-induced membrane damage: Hydroxyapatite crystal-induced hemolysis of erythrocytes. Biochem Med Metab Biol. 1986;36(1):25-35. doi: 10.1016/0885-4505(86)90103-9, PMID 3741700.
9. Han Y, Wang X, Dai H, Li S. Nanosize and surface charge effects of hydroxyapatite nanoparticles on red blood cell suspensions. ACS Appl Mater Interfaces. 2012;4(9):4616-22. doi: 10.1021/am300992x, PMID 22860897.
10. Aarthy S, Thenmuhil D, Dharunya G, Manohar P. Exploring the effect of sintering temperature on naturally derived hydroxyapatite for bio-medical applications. J Mater Sci Mater Med. 2019;30(2):21. doi: 10.1007/s10856-019-6219-9, PMID 30747333.
11. Hung IM, Shih WJ, Hon MH, Wang MC. The properties of sintered calcium phosphate with [Ca]/[P] = 1.50. Int J Mol Sci. 2012;13(10):13569-86. doi: 10.3390/ijms131013569, PMID 23202968.
12. Casella LA, Griesshaber E, Yin X, Ziegler A, Mavromatis V, Müller D, *et al*. Experimental diagenesis: Insights into aragonite to calcite transformation of *Arctica islandica* shells by hydrothermal treatment. Biogeosciences. 2017;14(6):1461-92. doi: 10.5194/bg-14-1461-2017.
13. Tee JK, Ong CN, Bay BH, Ho HK, Leong DT. Oxidative stress by inorganic nanoparticles. Wiley Interdiscip Rev Nanomed Nanobiotechnol. 2016;8(3):414-38. doi: 10.1002/wnan.1374, PMID 26359790.
14. Rocha JHG, Lemos AF, Agathopoulos S, Valério P, Kannan S, Oktar FN, *et al*. Scaffolds for bone restoration from cuttlefish. Bone. 2005;37(6):850-7. doi: 10.1016/j.bone.2005.06.018, PMID 16153899.
15. Kong J, Liu C, Yang D, Yan Y, Chen Y, Huang J, *et al*. Alv protein plays opposite roles in the transition of amorphous calcium carbonate to calcite and aragonite during shell formation. Cryst Growth Des. 2018;18(7):3794-804. doi: 10.1021/acs.cgd.8b00025.
16. Jensen ACS, Brif A, Pokroy B, Hinge M, Birkedal H. Morphology-preserving transformation of minerals mediated by a temperature-responsive polymer membrane: Calcite to hydroxyapatite. Cryst Eng Comm. 2016;18(13):2289-93. doi: 10.1039/C5CE02245B.
17. Karunagaran M, Murali P, Palaniappan V, Sivapathasundharam B. Expression and distribution pattern of podoplanin in oral submucous fibrosis with varying degrees of dysplasia–an immunohistochemical study. J Histotechnol. 2019;42(2):80-6. doi: 10.1080/01478885.2019.1594543.
18. Cozza N, Monte F, Bonani W, Aswath P, Motta A, Migliaresi C. Bioactivity and mineralization of natural hydroxyapatite from cuttlefish bone and Bioglass® co-sintered bioceramics. J Tissue Eng Regen Med. 2018;12(2):e1131-42. doi: 10.1002/term.2448, PMID 28500666.
19. Sarode SC, Gondivkar S, Gadbail A, Sarode GS, Yuwanati M. Oral submucous fibrosis and heterogeneity in outcome measures: A critical viewpoint. Future Oncol. 2021;17(17):2123-6. doi: 10.2217/fon-2021-0287, PMID 33858194.
20. Raj PD, Saravanan S, Shairam M, Selvakumar N, Selestin RI, Dhanasekaran A, *et al*. Bioactive zinc(II) complex incorporated PCL/gelatin electrospun nanofiber enhanced bone tissue regeneration. Eur J Pharm Sci. 2021;160:105768. doi: 10.1016/j.ejps.2021.105768, PMID 33607242.
21. Naga SM, El-Maghraby HF, Mahmoud EM, Talaat MS, Ibrhim AM. Preparation and characterization of highly porous ceramic scaffolds based on thermally treated fish bone. Ceram Int. 2015;41(10):15010-6. doi: 10.1016/j.ceramint.2015.08.057.
22. Jeevanandam J, Chan YS, Ku YH. Aqueous *Eucalyptus globulus* leaf extract-mediated biosynthesis of MgO nanorods. Appl Biol Chem. 2018;61(2):197-208. doi: 10.1007/s13765-018-0347-7.
23. Sroka-Bartnicka A, Borkowski L, Ginalska G, Ślósarczyk A, Kazarian SG. Structural transformation of synthetic hydroxyapatite under simulated *in vivo* conditions studied with ATR-FTIR-spectroscopic imaging. Spectrochim Acta A Mol Biomol Spectrosc. 2017;171:155-61. doi: 10.1016/j.saa.2016.07.051, PMID 27513683.
24. Hui P, Meena SL, Singh G, Agarawal RD, Prakash S. Synthesis of hydroxyapatite bio-ceramic powder by hydrothermal method. J Miner Mater Charact Eng. 2010;09(8):683-92. doi: 10.4236/jmmce.2010.98049.
25. Ivankovic H, Gallego Ferrer G, Tkalcec E, Orlic S, Ivankovic M. Preparation of highly porous hydroxyapatite from cuttlefish bone. J Mater Sci Mater Med. 2009;20(5):1039-46. doi: 10.1007/s10856-008-3674-0, PMID 19132509.
26. Venkatesan J, Kim SK. Effect of temperature on isolation and characterization of hydroxyapatite from tuna (*Thunnus obesus*) bone. Materials (Basel). 2010;3(10):4761-72. doi: 10.3390/ma3104761, PMID 28883351.
27. Yeoh FY. Synthesis and characterization of nanoporous hydroxyapatite with high hemocompatibility. BJSTR. 2018;5(4). doi: 10.26717/BJSTR.2018.05.001239.
28. Balu SK, Andra S, Jeevanandam J, S MV, V S. Emerging marine derived nanohydroxyapatite and their composites for implant and biomedical applications.

J Mech Behav Biomed Mater. 2021;119:104523. doi: 10.1016/j.jmbbm.2021.104523 , PMID 33940538.

29. Pellegrino ED, Biltz RM. Bone carbonate and the Ca to P molar ratio. Nature. 1968;219(5160):1261-2. doi: 10.1038/2191261a0, PMID 4971122.
30. Prithiviraj N, Yang GE, Thangavelu L, Yan J. Anticancer compounds from starfish regenerating tissues and their antioxidant properties on human oral epidermoid carcinoma KB cells. In: Pancreas. Two Commerce Sq, 2001 Market St, Philadelphia: Lippincott Williams and Wilkins. 2020;49:155-6.
31. Jiang L, Yu Y, Li Y, Yu Y, Duan J, Zou Y, *et al*. Oxidative damage and energy metabolism disorder contribute to the hemolytic effect of amorphous silica nanoparticles. Nanoscale Res Lett. 2016;11(1):57. doi: 10.1186/s11671-016-1280-5, PMID 26831695.
32. Chen LQ, Fang L, Ling J, Ding CZ, Kang B, Huang CZ. Nanotoxicity of silver nanoparticles to red blood cells: Size dependent adsorption, uptake, and hemolytic activity. Chem Res Toxicol. 2015;28(3):501-9. doi: 10.1021/tx500479m, PMID 25602487.

Cite this article: Dinesh Y, Balu SK, Ramalingam K, Ramani P. Biofabrication and Characterization using Egg Shell Nanoparticles and their Haemolytic Analysis: An *in-vitro* Study. Indian J of Pharmaceutical Education and Research. 2023;57(2s):s301-s306.